Smooth 3-D Reconstruction for 2-D Histological Images

Amalia Cifor[1], Tony Pridmore[1], and Alain Pitiot[2]

[1] School of Computer Science, University of Nottingham, Nottingham, UK
[2] Brain and Body Centre, University of Nottingham, Nottingham, UK
{rzc, tpp}@cs.nott.ac.uk, alain.pitiot@nottingham.ac.uk

Abstract. We present an image driven approach to the reconstruction of 3-D volumes from stacks of 2-D post-mortem sections (histology, cryoimaging, autoradiography or immunohistochemistry) in the absence of any external information. We note that a desirable quality of the reconstructed volume is the smoothness of its notable structures (e.g. the gray/white matter surfaces in brain images). Here we propose to use smoothness as a means to drive the reconstruction process itself.

From an initial rigid pair-wise reconstruction of the input 2-D sections, we extract the boundaries of structures of interest. Those are then evolved under a mean curvature flow modified to constrain the flow within 2-D planes. Sparse displacement fields are then computed, independently for each slice, from the resulting flow. A variety of transformations, from globally rigid to arbitrarily flexible ones, can then be estimated from those fields and applied to the individual input 2-D sections to form a smooth volume.

We detail our method and discuss preliminary results on both real histological data and synthetic examples.

1 Introduction

In spite of rapid advances in 3-D imaging technologies (high-field magnetic resonance scanners, micro-CT, etc.), the spatial resolution, contrast and specificity of the acquired volumes still fall short of the level of anatomical or functional details afforded by post-mortem 2-D imaging technologies such as histology, cryoimaging, autoradiography or immunohistochemistry (hereafter referred to as "histology").

By fusing 2-D post-mortem sections with 3-D in vivo or post-mortem volumes, we can establish a one-to-one correspondence between the various modalities, with the 3-D volumes acting as an adequate anatomical framework. This enables researchers to view the complex anatomy of the organs or structures of interest in three dimensions (regardless of the modality), at multiple scale (anatomical, cellular, molecular) and multiple explanatory levels (structural or functional).

Due to the nature and high incidence of the distortions and artefacts that occur during the 2-D imaging process (shape changes during perfusion, fixation and tissue extraction; holes and tears during cutting; nonlinear shrinking

J.L. Prince, D.L. Pham, and K.J. Myers (Eds.): IPMI 2009, LNCS 5636, pp. 350–361, 2009.

of tissues during preparation or dying; etc.) an accurate and robust fusion is difficult to achieve. The typical approach to fusion consists of (1) reconstructing a geometrically coherent 3-D volume by registering together the consecutive 2-D histological slices and (2) co-registering the reconstructed volume to the available 3-D modality (MR or CT for instance).

Often this first reconstruction involves registering successive pairs of 2-D slices with respect to a reference slice, generally taken as the middle one in the stack [1,2]. The available 2-D registration methods range from time-consuming manual techniques [3] or fiducial markers based ones [4], to more advanced geometrical approaches where features such as points [5], edges [6] or contours [7] are automatically extracted from the input slices. Iconic (i.e. intensity based) methods also proved very popular. For instance, Ourselin et al. [1] used a robust block-matching approach to linearly register histological sections of the rat brain with the correlation coefficient as similarity measure.

However, as argued at length in [2], restricting the reconstruction problem to a 2-D/2-D registration process is not likely to yield anatomically satisfactory results. Indeed, the 3-D conformation of a curved object is lost during the cutting process and cannot be accurately recovered in the absence of external information (the humorously nicknamed "banana problem"). Furthermore, considering slices only two at a time naturally gives rise to an aperture problem whose consequences are a general lack of robustness and a tendency to create wave patterns in the direction across slices.

Those issues can be alleviated in several ways. For instance, an external reference volume (e.g. MRI [8,2,9]) or the block-face images acquired during the histological process [10,11,12,13] can be used to guide the reconstruction. Recent approaches conjointly manipulate all the slices in the stack. In [14] for instance, the set of independent elastic transformations is globally optimized within a variational scheme, with the global sum of squared differences across all slices serving as fitness function. In [2], the linear transformations computed between each pairs of slices are filtered along the cutting axis. Yushkevitch et al. [15] use a graph-based approach to pick in the neighbourhood of each slice the registration path that will minimize the overall reconstruction error. In Guest et al.[16], springs are attached between corresponding points across consecutive slices, which are themselves modeled as thin elastic plates, and a finite element method evolves the system until equilibrium. In Tan et al. [17], three high-curvature points, extracted from tissue contours after an initial global reconstruction, are matched across slices and serve as surrogate fiducial markers. New affine transformations are estimated for each slice from the three displacement vectors computed between these feature points and the closest point in the same slice on an interpolating inter-slice cubic NURBS.

In this article, we focus on the reconstruction of a 3-D volume from 2-D slices, in the absence of an external reference. Indeed, the latter is not always available, or its resolution or contrast may not be sufficient to provide much help with the reconstruction. We note that a desirable quality for a reconstructed histological volume is the smoothness of its notable structures (e.g. the gray/white

matter surface in a brain). In fact, it is common practice to qualitatively evaluate a reconstruction method by considering the smoothness, in the reconstructed volume, of some structures of interest in views orthogonal to the original 2-D histological sections. For instance, in [14] the quality of reconstructed histological volumes of rat brains was assessed by an expert who visually evaluated both the smoothness of the borders delimiting anatomical structures and the amount of recognizable small structures, such as the subcortical nuclei and the ventricles. In [16,18], the distance between corresponding points identified across slices was used to quantify the smoothness of the reconstruction: since histological slices are thin, the closer the corresponding points, the smoother the volume. In a recent work [19], Laissue et al. use the smoothness of crest-lines defined by high curvature points of the lateral ventricle in a reconstructed histological brain to assess the co-registration errors between MRI and the reconstructed volume.

Here we propose to use smoothness as a means to drive the reconstruction itself. The boundaries of structures of interest are automatically extracted from an initial rigid reconstruction of the input 2-D sections and smoothed by a constrained mean curvature flow. Arbitrarily flexible transformations can then be estimated, independently for each slice, from the computed flow and applied to the original sections to form a smooth volume. We build our method around the hypothesis that the histological sections are sufficiently thin to enable a smooth visual aspect of the reconstructed structures in the direction across slices.

Note that our approach bears some resemblance to the work of Tan et al. [17], in the sense that we also use smoothness to correct slice transformations. However, instead of focusing on an arbitrarily small number of feature points which have to be extracted and matched across slices (an error-prone process highly sensitive to segmentation errors), we use actual surfaces. This enables us to estimate a displacement field instead of just three displacement vectors, so arbitrarily flexible slice transformations can be accommodated. In turn, this gives us control over the desired smoothness of the reconstructed volume.

We first detail our method in the following section, before presenting some preliminary results on synthetic and real datasets in section 3. Finally, we conclude with some elements of validation regarding the robustness of the proposed approach.

2 Method

Our method consists of five steps. (1) We first reconstruct an estimate of the 3-D histological volume by rigidly registering consecutive 2-D sections, using a classic pair-wise approach. (2) Structures of interest (e.g. the gray/white matter boundary) are automatically extracted from the reconstructed volume. (3) The extracted surfaces are smoothed by evolving them under a modified version of the mean curvature flow restricted to 2-D planes. (4) A 3-D displacement field is estimated from the 3-D flow. A variety of transformations, from globally rigid to arbitrarily flexible ones, can then be estimated from the field. (5) Finally, a smooth reconstructed volume is obtained by applying the transformations to the original 2-D slices.

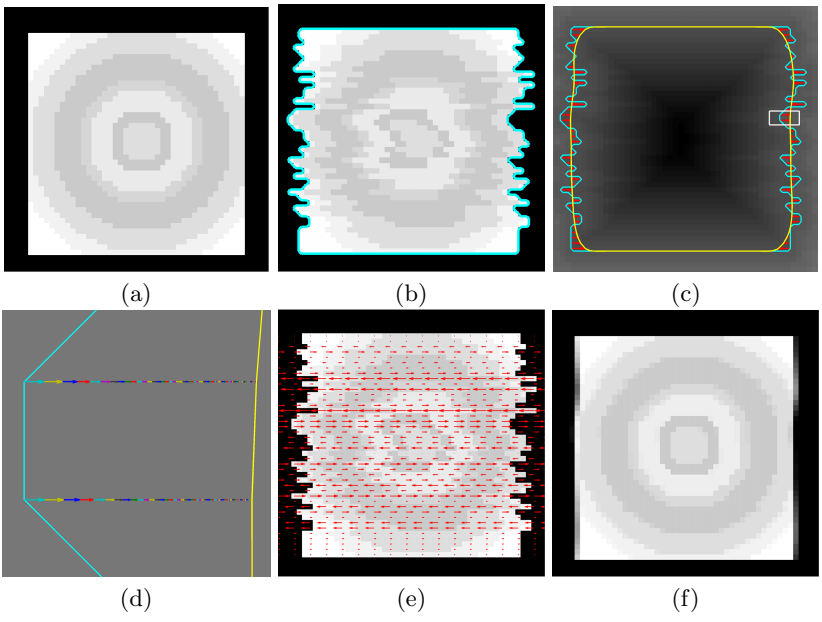

Fig. 1. Smooth reconstruction applied to a 2-D toy example: (a) source 2-D image: the structure of interest is a textured square; (b) source image after application of random translations to individual lines (gray) and extracted structure of interest (blue line); (c) signed distance map (gray), front before (blue line) and after (yellow line) application of flow, computed sparse displacement field (red); (d) magnified view of the trajectory of two points taken within the white square in (c) during the flow; (e) dense displacement field interpolated from the global rigid transformation (translations) estimated on sparse field of (c); (f) globally smoothed image

We illustrate on Fig. 1 the steps that will be described throughout this section. To facilitate visualization, we use a 2-D toy example rather than a 3-D one. The structure of interest is a textured square. In this example, the analogous of a 2-D histological slice is a horizontal line. We simulate the misalignments induced by the histological process by translating those lines horizontally by a random amount drawn from a zero-mean normal distribution (Fig. 1(b)). The goal of our approach is then to recover a smooth square, similar in shape to that of Fig. 1(a).

2.1 Approximating a 3-D Volume

We first need to estimate a globally coherent 3-D volume from the input stack of 2-D slices. We use the standard pair-wise reconstruction approach of Ourselin et al. [20], owing to its robustness to artifacts and noise. In this framework, consecutive pairs of 2-D slices are globally rigidly registered with a block-matching algorithm. We chose the middle slice as reference.

Note that any other global reconstruction approach could be used here (for instance, the robust approach of Yushkevich et al. [15] which would likely perform better if severe artifacts were to affect some sections).

As mentioned above, Fig. 1(b) simulates the 2-D image reconstructed from individual 1-D lines.

2.2 Extracting Structures of Interest

The roughness (as opposed to smoothness) of a reconstructed volume is usually best appreciated at the boundaries between visually homogeneous regions, which typically coincide with anatomical structures or sub-structures. Therefore, we propose to use the smoothness of a selection of boundaries as a proxy for the smoothness of the reconstructed volume. Note that because of the tessellated nature of histological slices, structures of interest can be found at a variety of scales. The decision as to which structure should be extracted is then informed by the overall goal of the application for which histological volume reconstruction is required.

An issue that interferes with the extraction of the boundaries is that of intensity inhomogeneities between sections. Those are mostly due to differences in staining densities, variations in slice thickness or the digitization stage of the image acquisition process. A number of solutions are available in the literature [21,22]. We picked the affine histogram matching approach of Malandain et al. [21] as it copes adequately with the anatomical differences and intensity variations across the stack of histological slices .

Once the intensities have been homogenized, we can extract the boundaries of the structures of interest. For the data presented in this paper, a simple intensity thresholding approach proved sufficient. Should the histological sections be more heavily textured, or if the noise level were higher, more sophisticated methods may become necessary. Note that the segmentation was done in 2-D, independently for each slice, which makes it independent from the quality of the initial 3-D reconstruction (although we may equally envision a 3-D segmentation approach). A completely accurate segmentation step is not mandatory here, since the extracted surfaces act as surrogates. Our method only requires approximately delineated boundaries of interest as long as their smoothness is representative for the smoothness of the initial volume reconstruction.

The blue line in Fig. 1(b) follows the boundary of the structure of interest in our toy example.

2.3 3-D Mean Curvature Flow Constrained to 2-D Planes

Because the initial rigid reconstruction is unlikely to generate a smooth volume, the extracted surfaces will be "jagged" in the direction of the cutting axis (i.e. across slices). We propose to smooth those surfaces by evolving them under a mean curvature flow.

Mean curvature flow is a popular interface motion method, extensively used as an image smoothing and noise filtering technique (see [23] for a review). At

a glance, it consists in moving each point on the extracted surfaces (or fronts) along their normal direction, with speed proportional to their curvature. This helps smoothing away their various kinks and bumps. An attractive formulation to the mean curvature flow was proposed by Osher et al. where the front was modelled implicitly as the zero level set of an higher dimensional function, a signed distance map [24]. Formally, if $\Gamma(t = 0)$ denotes the extracted front, then the level set function is $\phi(x, t = 0) = \pm distance(x, \Gamma(t = 0))$. If we further constrain the gradient of the signed distance function to be one, the general equation of motion [25] for speed function F is:

$$\phi_t + F \bigtriangledown \phi = 0 \tag{1}$$

When the speed is proportional to the curvature κ at each point, the equation becomes: $\phi_t + F(\kappa) \mid \bigtriangledown \phi \mid = 0$.

For the purpose of our histological reconstruction application, we modified this classical formulation to take into account the fact that the cutting axis (the axis going across slices) plays a different role from the other two, as argued in [2]. Indeed, we do not want the flow to go across the planes in which the slices reside since we need to compute from it the independent transformations to be applied to the original sections.

Restricting the flow to the planes can be simply obtained by setting the component of the velocity along the z-axis to zero. The speed function then becomes:

$$F(\kappa) = -b\kappa \cdot (1, 1, 0) \cdot (\frac{\bigtriangledown \phi}{\mid \bigtriangledown \phi \mid}) \tag{2}$$

where b is a positive constant. Plugging the new speed into the level set equation (1), the motion under the mean curvature flow constrained to the 2-D planes is given by:

$$\phi_t = [(b\kappa, b\kappa, 0) \cdot (\frac{\bigtriangledown \phi}{\mid \bigtriangledown \phi \mid})] \cdot \bigtriangledown \phi \tag{3}$$

Note that this formulation of the flow still allows for the curvature and gradient to be computed in 3-D. It also somewhat mitigates the tendency for classical mean curvature flows to shrink volumes, even though we cannot guarantee surface shrinkage within slices. In our study we used the Euclidean distance approximation for the signed distance map [26] and the derivatives in equation 3 are computed by means of second order centred differences[1].

2.4 Estimating Individual Slice Transformations

Finally, we need to compute the transformations corresponding to each individual slice. Once the equation of motion has been discretized, we can track, within each slice, the trajectory of the points on the evolving front and generate

[1] The described scheme was implemented on top of the LS Toolbox for matlab http://www.cs.ubc.ca/ mitchell/ToolboxLS/

a sparse displacement field. The transformation corresponding to each slice can then be estimated from this field.

However, since the original signed distance map does not remain a distance map throughout the entire time-period of the motion, finding an accurate set of displacement vectors from the points on initial front to the points on the final front is a difficult task. In [27] Gomes et al. recall that the characteristics of the level set function (the integral curves of its gradient) are straight lines since the embedding function is a distance map. They use a tracking approach to find the position of the front at each iteration. Inspired by this scheme, we too track the position of the front at each iteration by looking for zero-crossing of the distance map in the normal direction, starting at previous position of the front. The final displacement is obtained by composing the small displacement vectors at intermediary points between the old and new position of the front.

Fig. 1(c) shows the evolution of the front under our constrained mean curvature flow formulation and the computed sparse displacement field. Note how the displacement vectors are indeed aligned horizontally (i.e. the flow was restricted to the horizontal direction). Fig. 1(d) displays a magnified view of the trajectory, during the flow, of two points taken within the white square in (c).

Once a displacement field has been computed, we can estimate a variety of transformations, from globally rigid or affine ones to arbitrarily flexible ones. Following [1,28], we estimate global transformations with a robust least square regression algorithm (Least Trimmed Squares, [29]). This approach differs from standard least square methods in that it minimizes the sum of a certain percent of the smallest squared residuals in an iterative fashion, which reduces the influence of outliers. It proved particularly amenable to our application where only a sparse displacement field is computed. When more flexible transformations are desired, we use the rigidity adaptable approach of Pitiot et al. [28]. In this approach, both the geometry and topology of the individual slices are taken into account (in particular, image components on either side of a gap are treated independently). The flexibility of the regularized field is controlled by setting a single parameter, the rigidity radius, which determines the amount of local rigidity (the larger the radius, the more rigid the transformation). Finally, for maximal flexibility, we can extrapolate the sparse field to the entire image, where the extrapolation is done independently for each slice, and apply the displacement directly to the original slices.

Fig. 1(e) shows the dense displacement field interpolated along each line from the global rigid translation estimated from the sparse field shown in Fig. 1(c). Note that for this 2-D toy example, the global rigid translation of each line was obtained by averaging the displacement vectors computed on the line rather than by LTS since there were only two vectors. Fig. 1(f) shows the final 2-D image once the estimated translations were applied to the individual lines of Fig.1(b): the reconstructed image is visibly much smoother.

3 Results

3.1 Reconstructing a NISSL-Stained Volume of the C57BL/6 Mouse Brain

We applied our smooth reconstruction approach to a set of 350 Nissl-stained sections of the C57BL/6 mouse brain obtained from the LONI database[2]. The mouse brain was cut serially along the anterior/posterior axis in $50\mu m$ thick coronal sections.

Fig. 3(a) displays a sagittal (left) and transverse (right) view of the initial rigidly reconstructed volume (step 1 of our method). As mentioned above, we picked the middle section in the stack as reference for this pair-wise reconstruction. After the intensity homogenization step, we extracted the gray/white matter boundary as our surface of interest and subjected it to the modified mean curvature flow.

We show on Fig. 3(b to e) the reconstruction results obtained with increasingly more flexible transformation models. For all results, we used the same parameters for our mean curvature flow implementation: $b = 0.05$, 153 time steps in total.

The reconstruction obtained when global rigid transformations were estimated from our modified flow is shown in (b). Note how even though the transformations applied to the original sections were global rigid for both (a) and (b), the reconstructed volume appears much smoother with our approach. Without surprise, estimating a global affine transformation instead of a rigid one yielded a smoother volume (Fig. 3(c)).

Fig. 3(d) shows the reconstruction results obtained with the adaptive rigidity approach[28]. We chose a radius of the order of the cortical thickness in this area of the brain. The resulting volume compares favourably against that obtained when directly applying the displacement field computed from the flow (Fig. 3(e)). In both case we obtain a visually very smooth volume, but the regularization approach prevented the cortical ribbon from collapsing in the bottom left and top right corners of the image.

3.2 Elements of Robustness

In an attempt to evaluate the robustness of our smooth reconstruction method while circumventing the lack of ground truth associated with actual histological data, we propose to reconstruct a volume from the artificially perturbed slices of an initially smooth volume and compare the former with the latter. As surrogate for smooth histological volume, we use a high resolution 0.65mm isotropic in-vivo T1-weighted MR scan of the human brain of a volunteer. In a similar fashion to our toy 2-D example, we apply to each individual axial slice a rigid or affine transformation whose parameters are drawn from zero mean normal distributions of specifiable standard deviation σ.

Fig. 2 shows both coronal and sagittal views of the original, perturbed and smoothly reconstructed volumes for rotation drawn at random from a zero mean normal distribution of standard deviation $\sigma_{rotation} = 1$ degree (b) and

[2] http://map.loni.ucla.edu

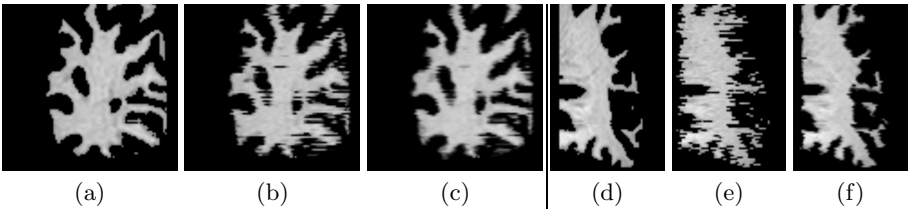

Fig. 2. Reconstructing a randomly perturbed MR image of the human brain: (a) coronal view of the original MRI; (b) coronal view of the perturbed MRI whose axial slices were randomly rotated ($\sigma_{rotation} = 1$ degree); (c) smooth reconstruction from slices rotated in (b); (d) sagittal view of the original MRI; (e) sagittal view of the perturbed MRI whose axial slices were randomly translated ($\sigma_{translation} = 2$ voxels); (f) smooth reconstruction from slices translated in (e).

translations drawn at random from a zero mean normal distribution of standard deviation $\sigma_{translation} = 2$ voxels (e). The reconstructed volumes (c and f) are indeed much smoother than the perturbed volumes and visually close to the original MRI. Note that because our reconstruction approach does not know about brain anatomy, there is no guarantee that the "smooth alignment" corresponds to the anatomically correct one. In particular, it could be smoother.

4 Conclusions

We have presented a reference-free image driven approach to volume reconstruction where smoothness is used as a means to drive the reconstruction process itself. A variant of the mean curvature flow constrained to 2-D planes is used to smooth the boundaries of structures of interest extracted from an initial reconstruction of the input histological sections. A displacement field is then computed from the resulting flow and arbitrarily flexible transformations are estimated and applied to the individual slices.

Preliminary results indicate that the reconstructed volumes are indeed visually smooth, even when the selected slice transformation model is globally rigid.

Note that our method is best suited for histological slices in which the discrepancy between boundaries of interest and texture is high enough to extract and smooth these boundaries. We are currently investigating the influence of noise and lack of contrast on the quality of the reconstruction and quantifying the robustness of our approach to random rotations and translations. We are evaluating volume preserving flows to further improve the quality of the reconstruction. Of particular interest are scale-dependent flows which would smooth out only those features artificially induced by the reconstruction, while leaving the overall shape of the structure intact.

Acknowledgements

This research is funded by the European Commission Fp6 Marie Curie Action Programme (MEST-CT-2005-021170).

References

1. Ourselin, S., Roche, A., Subsol, G., Pennec, X., Ayache, N.: Reconstructing a 3D structure from serial histological sections. Image and Vision Computing 19(1-2), 25–31 (2001)
2. Malandain, G., Bardinet, E., Nelissen, K., Vanduffel, W.: Fusion of autoradiographs with an MR volume using 2-D and 3-D linear transformations. NeuroImage 23(1), 111–127 (2004)
3. Deverell, M., Salisbury, J., Cookson, M., Holman, J., Dykes, E., Whimster, F.: Three-dimensional reconstruction: methods of improving image registration and interpretation. In: Analytical Cellular Pathology, vol. 5, pp. 253–263 (1993)
4. Toga, A., Goldkorn, A., Ambach, K., Chao, K., Quinn, B., Yao, P.: Postmortem cryosectioning as an anatomic reference for human brain mapping. Computerized Medical Imaging and Graphics 21(11), 131–141 (1997)
5. Guest, E., Berry, E., Baldock, R.A., Fidrich, M., Smith, M.A.: Robust point correspondence applied to two-and three-dimensional image registration. IEEE Trans. Pattern Anal. Mach. Intell. 23(2), 165–179 (2001)
6. Kim, B., Frey, K.A., Mukhopadhayay, S., Ross, B.D., Meyer, C.R.: Co-registration of MRI and autoradiography of rat brain in three-dimensions following automatic reconstruction of 2D data set. In: Ayache, N. (ed.) CVRMed 1995. LNCS, vol. 905, pp. 262–266. Springer, Heidelberg (1995)
7. Cohen, F., Yang, Z., Huang, Z., Nissanov, J.: Automatic matching of homologous histological sections. IEEE Transactions on Bio-medical Engineering 445(5), 642–649 (1998)
8. Ourselin, S., Bardinet, E., Dormont, D., Malandain, G., Roche, A., Ayache, N., Tande, D., Parain, K., Yelnik, J.: Fusion of histological sections and MR images: towards the construction of an atlas of the human basal ganglia. In: Niessen, W.J., Viergever, M.A. (eds.) MICCAI 2001. LNCS, vol. 2208, pp. 743–751. Springer, Heidelberg (2001)
9. Chakravarty, M.M., Bedell, B.J., Zehntner, S.P., Evans, A.C., Collins, D.L.: Three-dimensional reconstruction of serial histological mouse brain sections. In: ISBI, pp. 987–990 (2008)
10. Dauguet, J., Delzescaux, T., Condé, F., Mangin, J.F., Ayache, N., Hantraye, P., Frouin, V.: Three-dimensional reconstruction of stained histological slices and 3D non-linear registration with in-vivo MRI for whole baboon brain. Journal of Neuroscience Methods 164, 191–204 (2007)
11. Gefen, S., Tretiak, O., Nissanov, J.: Elastic 3D alignment of rat brain histological images. IEEE Transactions on Medical Imaging 22(11), 1480–1489 (2003)
12. Bardinet, E., Ourselin, S., Dormont, D., Malandain, G., Tandé, D., Parain, K., Ayache, N., Yelnik, J.: Co-registration of histological, optical and MR data of the human brain. In: Dohi, T., Kikinis, R. (eds.) MICCAI 2002. LNCS, vol. 2488, pp. 548–555. Springer, Heidelberg (2002)
13. Kim, B., Boes, J., Frey, K., Meyer, C.: Mutual information for automated unwarping of rat brain autoradiographs. NeuroImage 5(1), 31–40 (1997)
14. Wirtz, S., Fischer, B., Modersitzki, J., Schmitt, O.: Super–fast elastic registration of histologic images of a whole rat brain for three–dimensional reconstruction. In: Proceedings of SPIE 2004, Medical Imaging, vol. 5730, pp. 14–19 (2004)
15. Yushkevich, P.A., Avants, B.B., Ng, L., Hawrylycz, M., Burstein, P.D., Zhang, H., Gee, J.C.: 3D mouse brain reconstruction from histology using a coarse-to-fine approach. In: Pluim, J.P.W., Likar, B., Gerritsen, F.A. (eds.) WBIR 2006. LNCS, vol. 4057, pp. 230–237. Springer, Heidelberg (2006)

16. Guest, E., Baldock, R.: Automatic reconstruction of serial sections using the finite element method. BioImaging 3, 154–167 (1995)
17. Tan, Y., Hua, J., Dong, M.: Feature curve-guided volume reconstruction from 2D images. In: Proceedings of International Symposium on Biomedical Imaging, April 2007, pp. 716–719 (2007)
18. Ju, T., Warren, J., Carson, J., Bello, M., Kakadiaris, I., Chiu, W., Thaller, C., Eichele, G.: 3D volume reconstruction of a mouse brain from histological sections using warp filtering. Journal of Neuroscience Methods 156, 84–100 (2006)
19. Laissue, P., Kenwright, C., Hojjat, A., Colchester, A.C.F.: Using curve-fitting of curvilinear features for assessing registration of clinical neuropathology with in vivo MRI. In: Metaxas, D., Axel, L., Fichtinger, G., Székely, G. (eds.) MICCAI 2008, Part II. LNCS, vol. 5242, pp. 1050–1057. Springer, Heidelberg (2008)
20. Ourselin, S., Roche, A., Prima, S., Ayache, N.: Block matching: A general framework to improve robustness of rigid registration of medical images. In: Delp, S.L., DiGoia, A.M., Jaramaz, B. (eds.) MICCAI 2000. LNCS, vol. 1935, pp. 557–566. Springer, Heidelberg (2000)
21. Malandain, G., Bardinet, E.: Intensity Compensation within Series of Images. In: Ellis, R.E., Peters, T.M. (eds.) MICCAI 2003. LNCS, vol. 2879, pp. 41–49. Springer, Heidelberg (2003)
22. Dauguet, J., Mangin, J.F., Delzescaux, T., Frouin, V.: Robust inter-slice intensity normalization using histogram scale-space analysis. In: Barillot, C., Haynor, D.R., Hellier, P. (eds.) MICCAI 2004. LNCS, vol. 3216, pp. 242–249. Springer, Heidelberg (2004)
23. Suri, J.S., Liu, K., Singh, S., Laxminarayan, S., Zeng, X., Reden, L.: Shape recovery algorithms using level sets in 2-d/3-d medical imagery: a state-of-the-art review. IEEE Transactions on Information Technology in Biomedicine 6(1), 8–28 (2002)
24. Osher, S.J., Fedkiw, R.P.: Level Set Methods and Dynamic Implicit Surfaces. Springer, Heidelberg (2002)
25. Osher, S., Sethian, J.A.: Fronts propagating with curvature-dependent speed: Algorithms based on Hamilton-Jacobi formulations. Journal of Computational Physics 79, 12–49 (1988)
26. Borgefors, G.: On digital distance transforms in three dimensions. Computer Vision and Image Understanding 64(3), 368–376 (1996)
27. Gomes, J., Faugeras, O.D.: Level sets and distance functions. In: Vernon, D. (ed.) ECCV 2000. LNCS, vol. 1842, pp. 588–602. Springer, Heidelberg (2000)
28. Pitiot, A., Guimond, A.: Geometrical regularization of displacement fields for histological image registration. Medical Image Analysis 12(1), 16–25 (2008)
29. Rousseeuw, P.J.: Least median of squares regression. Journal of the American Statistical Association 79(388), 871–880 (1984)

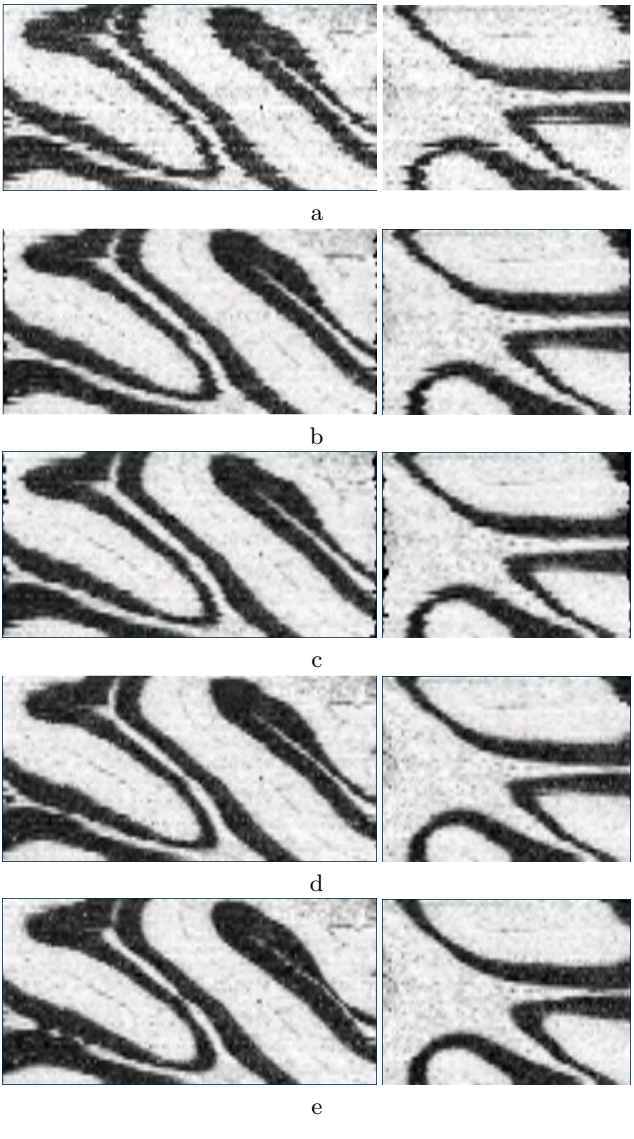

Fig. 3. Sagittal (left) and transversal (right) views of the LONI C57BL/6 mouse brain reconstructed from 2-D Nissl-stained sections using: (a) pair-wise globally rigid reconstruction; (b) smooth reconstruction approach with globally rigid transformations estimated at each slice. (c) same with globally *affine* transformations estimated at each slice. (d) same with rigidity adaptable regularization of the displacement field extracted from the flow; (e) same with direct application of the displacement field extracted from the flow.